NUCLEUS
2023, VOL. 14, NO. 1, 2202548
https://doi.org/10.1080/19491034.2023.2202548

Taylor & Francis
Taylor & Francis Group

RESEARCH ARTICLE

Lamin B1 overexpression alters chromatin organization and gene expression

Jeanae M. Kaneshiro[a], Juliana S. Capitanio[a,b], and Martin W. Hetzer[a,c]

[a]Molecular and Cell Biology Laboratory, Salk Institute for Biological Studies, La Jolla, CA, USA; [b]Paul F. Glenn Center for Biology of Aging Research, Salk Institute for Biological Studies, La Jolla, CA, USA; [c]Institute of Science and Technology Austria, Klosterneuburg, Austria

ABSTRACT

Peripheral heterochromatin positioning depends on nuclear envelope associated proteins and repressive histone modifications. Here we show that overexpression (OE) of Lamin B1 (LmnB1) leads to the redistribution of peripheral heterochromatin into heterochromatic foci within the nucleoplasm. These changes represent a perturbation of heterochromatin binding at the nuclear periphery (NP) through a mechanism independent from altering other heterochromatin anchors or histone post-translational modifications. We further show that LmnB1 OE alters gene expression. These changes do not correlate with different levels of H3K9me3, but a significant number of the misregulated genes were likely mislocalized away from the NP upon LmnB1 OE. We also observed an enrichment of developmental processes amongst the upregulated genes. ~74% of these genes were normally repressed in our cell type, suggesting that LmnB1 OE promotes gene de-repression. This demonstrates a broader consequence of LmnB1 OE on cell fate, and highlights the importance of maintaining proper levels of LmnB1.

ARTICLE HISTORY
Received 23 November 2022
Revised 10 April 2023
Accepted 11 April 2023

KEYWORDS
Chromatin organization; gene expression; nuclear lamina; nuclear envelope; heterochromatin

Introduction

Chromatin is highly organized within the nucleus, with heterochromatin at the nuclear periphery (NP) and euchromatin in the nucleoplasm [1]. Altered heterochromatin distribution has been observed in specific cell types, age, and disease, raising the question of what mediates proper heterochromatin organization within the nucleus [2–6].

The nuclear envelope (NE) associated proteins, including lamins and inner nuclear membrane proteins, are important for proper heterochromatin tethering at the NP. These proteins serve as anchors that bind heterochromatin either directly or indirectly through adaptor proteins, such as Heterochromatin Protein 1 (HP1), and depletion of these proteins generally perturbs peripheral heterochromatin localization [7–15]. Recently, cell-type specific heterochromatin anchors that function in tethering cell-type specific genes at the periphery have also been discovered [16–18]. This suggests that modulating the NE associated proteome can impact chromatin organization, and this may have a broader significance in the context of cell fate.

Histone post-translational modifications (PTMs) are also crucial in heterochromatin organization. A classic marker of peripheral heterochromatin is the di- and tri-methylation of Histone H3 on Lysine 9 (H3K9me2/3), and its deposition by several lysine methyltransferases is required for heterochromatin positioning at the NP [19–21]. Depletion of these heterochromatin marks correlates with the loss of peripheral heterochromatin, representing another key factor in proper chromatin organization within the nucleus [22–24].

Further, transcription and chromatin compaction are involved in heterochromatin positioning at the NP. For example, artificially induced transcription or chromatin decondensation of peripherally associated genes relocalizes them into the nuclear interior [25,26]. Conversely, reduced transcription can increase gene contact with the NP [25]. Collectively, these examples describe important mediators of heterochromatin organization that must be tightly regulated to establish conventional chromatin patterning within the nucleus.

Here, we present an interesting phenomenon in which overexpression (OE) of the NE associated protein Lamin B1 (LmnB1) alters chromatin organization such that peripheral heterochromatin is lost and heterochromatic DNA foci form within the nucleoplasm. Similar

CONTACT Martin W. Hetzer martin.hetzer@ist.ac.at Molecular and Cell Biology Laboratory, Salk Institute for Biological Studies, La Jolla, CA 92037, USA
Supplemental data for this article can be accessed online at https://doi.org/10.1080/19491034.2023.2202548

changes in chromatin organization upon LmnB1 OE have been previously reported but were shown to be a consequence of reduced Lap2 expression or senescence induction [27,28]. LmnB1 OE has also been shown to induce senescence in a separate study, however it was demonstrated that LmnB1 OE-induced senescence is incompatible with hTERT expression [29].

In our study utilizing RPE1 cells immortalized with hTERT, we observed that these heterochromatin foci can form independently from senescence. Additionally, LmnB1 OE does not seem to reduce the expression of other NE associated proteins or histone methylation marks important in peripheral heterochromatin tethering. This suggests a unique mechanism involved in these changes in chromatin organization. Given that LmnB1 is highly expressed in specific types of cancer (e.g. hepatocellular carcinoma, lung adenocarcinoma, clear-cell renal cell carcinoma) and certain neurological diseases (e.g. adult-onset autosomal dominant leukodystrophy, ataxia telangiectasia) [27,30–35], we explored the consequences of LmnB1 OE-induced chromatin reorganization on gene expression. We identified >100 misregulated genes and observed that many genes become de-repressed upon LmnB1 OE.

Materials and methods

Cell culture and stable cell lines

RPE1 cells were cultured in DMEM/F12 with 10% fetal bovine serum, 1% penicillin-streptomycin, and 0.01 mg/mL hygromycin B. IMR90 cells were cultured in DMEM with 10% fetal bovine serum, 1% penicillin-streptomycin, 1% NEAA, and 1% glutaMAX.

The pLVXTP plasmid backbone used for stable cell-line production was derived from the pLVX-UbC-rtTA-Ngn2:2A:EGFP plasmid, a gift from Fred Gage (Addgene plasmid # 127288; http://n2t.net/addgene:127288; RRID:Addgene_127288) [36]. The Ngn2:2A:EGFP insert was removed using Not1 and EcoR1 restriction enzymes, and In-Fusion cloning was used to insert mCherry, or mCherry tagged LmnB1 (NM_005573), LmnB1-ΔCaaX (NM_005573 with a four amino acid deletion (Cys, Ala, Ile, and Met) prior to the stop codon), or Lap2β (NM_001032283). Stable cell lines were produced according to the Addgene lentivirus production protocol using 293T cells (https://www.addgene.org/protocols/lentivirus-production/). RPE1 and IMR90 cells were infected and selected with puromycin for 10 days. Clonal lines in RPE1 cells were established by isolating single cells in 96 well plates. Two clonal lines for each overexpression construct were utilized for downstream analyses. About 0.05 ug/mL of doxycycline was used to induce OE of each construct.

Antibodies

Lamin B1 (sc -56,144; IF 1:250) and Lap2 (sc -28,541; IF 1:500; WB 1:1000) antibodies were purchased from Santa Cruz Biotechnology; Lamin A (L1293; IF 1:1000; WB 1:1000) antibody was purchased from Sigma-Aldrich; LBR (12398–1-AP; IF 1:100; WB 1:1000) antibody was purchased from Thermo Fisher Scientific; HP1α (#2616; IF 1:200; WB 1:1000), H3K27me3 (#9733; IF 1:1600), and β-actin (#3700; WB 1:1000) antibodies were purchased from Cell Signaling Technology; H3K9me3 (ab8898; IF 1:500; WB 1:1000; Cut&Run 1:100) antibody was purchased from Abcam; H3K9me2 (#39041; IF 1:500; WB 1:2000) antibody was purchased from Active Motif; GAPDH (MAB5718; WB 1:5000) antibody was purchased from R&D Systems.

Immunofluorescence microscopy

Cells were grown on coverslips and fixed with 4% PFA in 1× PBS for 5 minutes at room temperature. Coverslips were blocked with an IF buffer (10 mg/mL BSA, 0.1% Triton-X-100, 0.02% SDS, diluted in 1× PBS) for 20 minutes prior to incubation with primary and secondary antibodies diluted in the IF buffer. Coverslips were briefly incubated with Hoechst (1 µg/mL, Molecular Probes) and mounted with Vectashield (Vector Labs). The imaging was performed on a Leica SP8 confocal microscope with a 63 × 1.4NA oil immersion objective. Fiji was used to quantify the fluorescence intensity of LmnB1 and generate plot profiles representing the colocalization of DNA with markers of SAHF. LmnB1 fluorescence intensity

values were normalized to the average fluorescence intensity observed in the mCherry stable cell lines. Line scans were typically generated through the minor axis of individual nuclei. However, in cells overexpressing LmnB1, axes were chosen based on the localization of the induced DNA foci. For RPE1 clonal cell lines, two clonal lines for each OE construct were analyzed, with two biological replicates ($n = 4$), unless otherwise specified in the figure legend. For IMR90 cell lines, three biological replicates were performed ($n = 3$).

Electron microscopy

Cultured cells were prepared by electron microscopy as previously reported [37]. Briefly, the cells were cultured to approximately 70% confluence in 10 cm dishes. The medium was gently poured out and ~ 1 mL of 2.5% glutaraldehyde in 100 mM cacodylate buffer with 3 mM $CaCl_2$ (cacodylate buffer) prewarmed to 37°C was gently added and swirled. Approximately 5 mL of ice-cold fixative was gently added to the dish, and cells were fixed on ice for 30 min. Cells were washed with ice-cold cacodylate buffer three times before staining for 45 minutes with 1.5% osmium tetroxide reduced with 1.5% potassium ferrocyanide in cacodylate buffer at room temperature in the dark. Dishes were rinsed with ice-cold water three times before cells were released from the dishes using cell scrapers and pelleted in Eppendorf tubes for further processing.

Cell pellets were stained with 1% uranyl acetate overnight at 4°C and washed with ice-cold water three times. Cells were serially dehydrated by changes in ice-cold solutions of increasing ethanol concentrations, followed by two incubations for 45 minutes in anhydrous ethanol at room temperature. The cells were then infiltrated with Epon 812 (Electron Microscopy Sciences) and embedded in their Eppendorf tubes. Ultrathin sections (60 nm) were collected for each cell line using diamond knives (Diatome) on an ultramicrotome (Leica UC7), and imaging was performed on a Carl Zeiss Libra 120kV PLUS energy filtered transmission electron microscope.

Heterochromatin height at the NP was quantified using Fiji. Measurements were taken perpendicular to the nuclear membrane, and the maximum height was recorded every 100 nm. A total of 11 µm of NE was assessed, and only regions where the double membrane could be clearly visualized were included.

CellEvent senescence green detection kit

The RPE1 cells were cultured with doxycycline for 9 days, or treated with doxorubicin (500 nM) for 48 hours, followed by PBS washout and culturing for 9 days before collection. Cells were seeded into ibidi 8 well chambers one day prior to senescence detection using the CellEvent senescence green detection kit (Thermo Fisher Scientific). Samples were prepared according to the manufacturer's protocol. More than 50 cells were visualized in each cell line, with one clonal line overexpressing mCherry and two clonal lines overexpressing LmnB1. Two biological replicates were analyzed for each cell line.

Click-It EdU imaging kit

Cells were grown on coverslips and arrested in the 1/S phase using 3 µM of aphidicolin for 24 hours, followed by incubation with doxycycline and 10 µM of EdU for an additional 24 hours post-aphidicolin treatment. Coverslips were prepared according to the Click-iT EdU fluorescence detection protocol (Thermo Fisher Scientific) and imaged on a Leica SP8 confocal microscope with a 63 × 1.4NA oil immersion objective. More than 50 cells were visualized in two clonal cell lines for each OE construct, with two biological replicates for each cell line.

Western blotting

Cells were lysed in RIPA buffer (50 mM Tris-HCl, 150 mM NaCl, 1% Triton-X, 0.5% Sodium Deoxycholate, and 0.1% SDS), and protein concentrations were normalized using the BCA protein assay (Thermo Fisher Scientific). Membranes were blocked using 5% nonfat milk in 1× TBST for 15 min prior to incubation, with primary and secondary antibodies diluted in a blocking buffer. Secondary antibodies were conjugated to HRP for detection. Two clonal cell lines for each OE

construct were analyzed, with two biological replicates.

mRNA-sequencing

The RPE1 cells were treated with doxycycline for 24 hours and RNA was isolated using Trizol (Ambion) and purified with the RNeasy kit (Qiagen). RNA was shipped to Novogene for mRNA library preparation and run on the Illumina NovaSeq system (paired end 150). Samples include two clonal cell lines for each OE construct, with three biological replicates for each cell line ($n = 6$). After quality check (fastQC; https://www.bioinformatics.babraham.ac.uk/projects/fastqc/), trimming (TrimGalore used for removal of adapter and low-quality bases; https://www.bioinformatics.babraham.ac.uk/projects/trim_galore/), removal of genome contaminants (BBSplit; http://sourceforge.net/projects/bbmap/) and ribosomal RNA (SortMeRNA [38], fastq reads were aligned to the human reference sequence GRCh38 (hg38) and annotated with the corresponding gencode GTF file (gencode v38 primary assembly annotation) using the genome aligner STAR [39]. Duplicate reads were marked with Picard Toolkit (https://broadinstitute.github.io/picard/) and read counts per gene were quantified using Salmon [40]. Per gene read counts were normalized using DESeq2, this normalization method finds the ratio of each count to the geometric mean of all counts for that gene across all samples. The median of these ratios (size factor) per sample is used for its scaling. After filtering out low-expression genes (less than 10 counts total across all samples), differential expression was assessed using DESeq2 negative binomial generalized linear models [41], with differentially expressed genes defined as those with an adjusted p-value <0.05 and a log2 fold change >1 or <−1. De-repressed genes were defined as those with less than 100 normalized mRNA counts in the RPE1 mCherry stable cell lines but upregulated upon LmnB1 OE. Gene ontology biological processes enrichment analysis was used for downregulated, upregulated, and de-repressed genes (Bioconductor package clusterProfiler [42]. For the downregulated and upregulated genes, the top 10 unique biological processes are reported, with adjusted p-values <0.01. For the 'de-repressed genes', a subset of the top 30 unique biological processes are reported in the figure, with adjusted p-values <0.05. All of the biological processes with adjusted p-values for these 'de-repressed genes' are reported in Supplemental Table S2.

Cut&run-sequencing

The RPE1 cells were treated with doxycycline for 24 hours and 500,000 cells were harvested for each sample. Samples include two clonal cell lines for each OE construct, with two technical replicates. The H3K9me3 antibody (ab8898) was diluted 1:100 in antibody-binding buffer. Cut&Run was performed according to the EpiCypher CUTANA protocol, with the following exceptions. CUTANA H3K4 MetStat Spike-in Control dNucs were not added during antibody binding (Section IV). *E. coli* Spike-in DNA was diluted 1:10 prior to addition after chromatin digestion (Section VI).

Purified Cut&Run DNA was prepared for sequencing using the NEBNext Ultra II Library Kit Prep for Illumina, according to the manufacturer's protocol. About 15 µL of Cut&Run DNA was used for the mCherry samples, and 8 µL of Cut&Run DNA was used for the LmnB1 samples. Adapters were diluted 1:15 prior to adapter ligation. About 4 uL of i7 and i5 primers combined were used for PCR amplification. Libraries were sequenced on the Illumina NextSeq platform (paired end 75).

After quality check (fastQC; https://www.bioinformatics.babraham.ac.uk/projects/fastqc/) reads were trimmed (TrimGalore; https://www.bioinformatics.babraham.ac.uk/projects/trim_galore/) and aligned to the human genome, hg38, with BWA [43]. Duplicate reads were marked with Picard Toolkit (https://broadinstitute.github.io/picard/) and filtered out if meeting any of the following criteria (applied to forward and reverse pair-end reads): reads mapping to ENCODE's blacklist, marked as duplicates, not uniquely aligned, or with pairs in the wrong orientation or distance/chromosome [44,45]. For visualization, bigwig tracks were created using deeptools (bamCoverage) [46]. Peaks were called using epic2 (bin size 1000, gaps allowed 3 [47]; with input control). DiffBind [48] was used to investigate the differential deposition of H3K9me3 in cells overexpressing mCherry versus LmnB1; no regions of

differential H3K9me3 were observed with an adjusted p-value <0.05. Peaks were annotated using HOMER [49] and the Bioconductor package ChIPseeker [50]. FeatureCounts (Rsubread Bioconductor package [51]; was used to count reads from H3K9me3 Cut&Run at genes and promoter regions. The read counts were normalized using DESeq2's scaling method as described in the mRNA sequencing section above. Genes were called within H3K9me3 peaks if H3K9me3 marked the transcription start site (TSS), the promoter (<3kb from the TSS), or the gene body.

DamID-sequencing analysis

Previously published LmnB1 DamID datasets in RPE1 cells were obtained from the 4D Nucleome Data Repository [52]4DNFIMZGJCYC and 4DNFIRDCJXYU). Peaks were filtered for only those present in all replicates using bedtools [53] and annotated with ChIPseeker [50]. Genes bound by LmnB1 were called if they overlapped with LmnB1-DamID peaks in both replicates and if the LmnB1-DamID peaks overlapped with the TSS or the promoter (<3kb from the TSS). A hypergeometric test was used to determine the significance of the overlap between differentially expressed genes with H3K9me3 peaks, LmnB1 peaks, or both peaks (Bioconductor package GeneOverlap) [53].

Statistical analysis

Normality and Mann Whitney tests (two-sided) were performed using GraphPad Prism. Hypergeometric test (two-sided) was performed in RStudio. All p-values were adjusted for multiple comparisons when needed.

Data availability

RNA-sequencing and Cut&Run-sequencing data are available on GEO: GSE212110.

Results and discussion

Lamin B1 overexpression alters heterochromatin organization

A growing list of human disorders, including cancer, has been linked to misexpression of LmnB1 [27,30,32,33,35]. To specifically study the functional consequences of LmnB1 OE, we established two cell lines, RPE1 and IMR90, containing stably integrated doxycycline-inducible OE of mCherry tagged LmnB1. Immunofluorescence imaging revealed that doxycycline induction increases LmnB1 expression ~twofold, which is within the range of what has been previously reported in specific types of cancers with high levels of LmnB1 [32,35,54]. Furthermore, we observed that LmnB1 OE coincides with changes in chromatin organization, such that punctate DNA foci form within the nucleus (Supplemental Figure S1A, S1B). This was evident in >80% of the cells overexpressing LmnB1 and was not observed upon OE of LmnB1-ΔCaaX, which is a four amino acid deletion mutant of LmnB1 that prevents its post-translational processing and insertion into the NE. Additionally, these changes were not observed upon OE of Lap2β, an inner nuclear membrane protein that interacts with LmnB1. Importantly, this phenotype was observed in both RPE1 and IMR90 cells, despite RPE1 cells being near-diploid and immortalized with hTERT. This demonstrates that LmnB1 must be properly processed and overexpressed at the NE to elicit these changes in chromatin organization.

We next characterized the DNA foci formed upon OE of LmnB1. Using immunofluorescence imaging, we observed that the DNA foci is colocalized with H3K9me3 (Figure 1a). Furthermore, this colocalization was detected in every cell that exhibited these changes in chromatin organization induced by LmnB1 OE (70/70 nuclei). We also noticed a concurrent reduction of H3K9me3 signal at the NP, which was restored within 24 hours of doxycycline removal (Supplemental Figure S2). Additionally, we confirmed that LmnB1 expression was reduced at this 24-hour timepoint (Supplemental Figure S2). This suggests that LmnB1 OE may preclude the localization of heterochromatin at the NP, leading to the aberrant formation of heterochromatic foci within the nucleoplasm.

To confirm the changes in peripheral heterochromatin we detected by immunofluorescence imaging, we processed these cells for transmission electron microscopy (TEM), where heterochromatin can be clearly visualized as electron-dense

signals beneath the NE (Figure 1b, arrowheads). Complementary to what we observed with immunofluorescence (Figure 1a), TEM imaging displayed a strong reduction or loss of peripheral heterochromatin upon LmnB1 OE (Figure 1b). Further, measurements of heterochromatin height at the NP were significantly decreased in cells overexpressing LmnB1. Taken together, our data

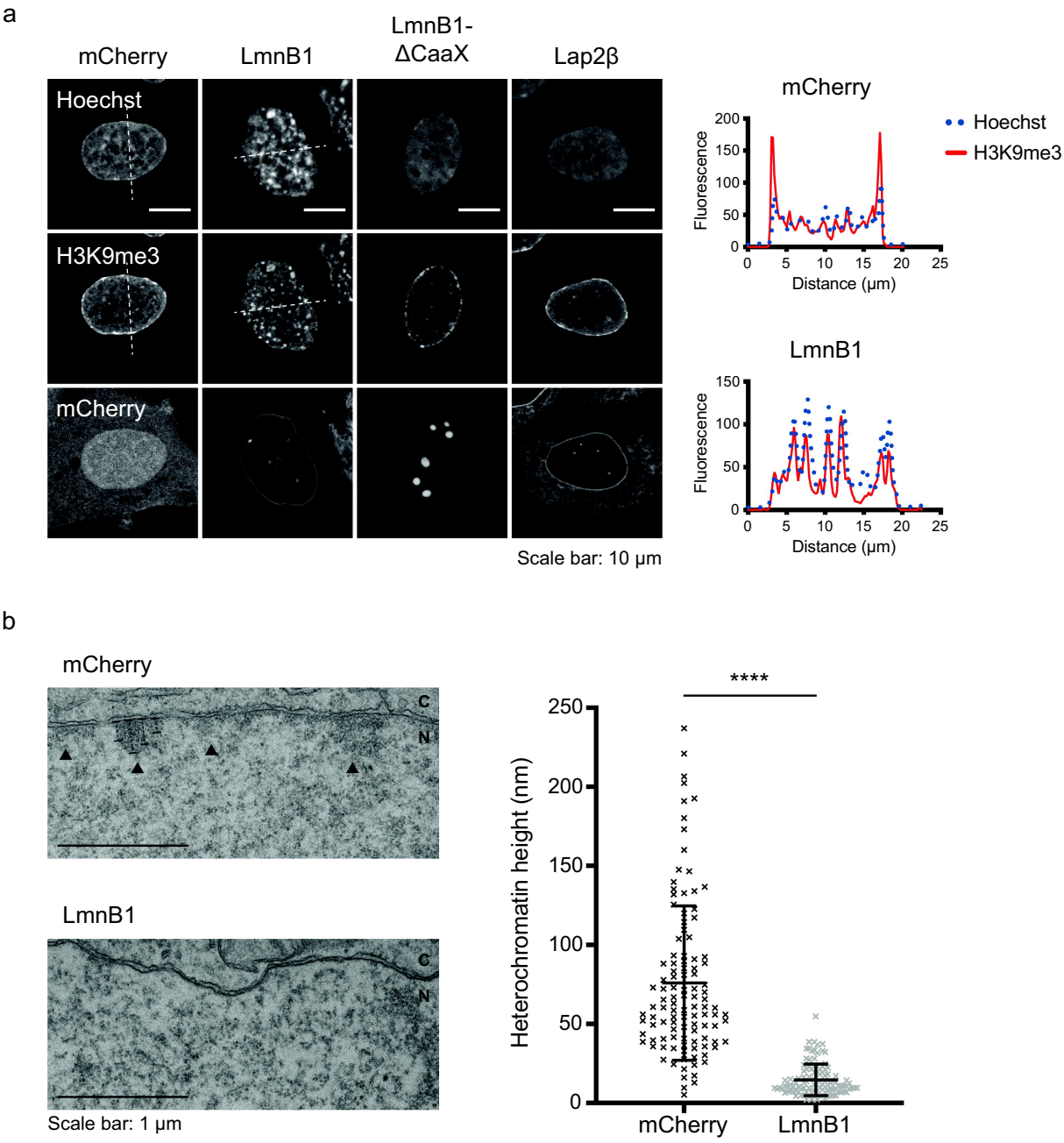

Figure 1. Lamin B1 overexpression alters heterochromatin localization at the nuclear envelope. (a) Representative confocal images of RPE1 stable cell lines treated with doxycycline for 24 hours and labeled with H3K9me3. Single z slices through the center of the nucleus are shown. Plot profiles on the right illustrate the overlap of fluorescence signal between DNA (Hoechst) and H3K9me3 over the white dotted lines in the mCherry and LmnB1 stable cell line images. 70/70 nuclei exhibited colocalization between H3K9me3 and the DNA foci in cells overexpressing LmnB1. (b) Representative transmission electron microscopy images of RPE1 stable cell lines treated with doxycycline for 24 hours. Arrowheads indicate heterochromatin lining the nuclear envelope. Dotted lines represent example measurements taken. The maximum height of heterochromatin perpendicular to the inner nuclear membrane was measured every 100 nm, over a total length of 11 μm, and is plotted on the right. Error bars indicate the mean ± standard deviation. Mann Whitney test for statistical significance: **** $p < 0.0001$. C = cytoplasm; N = nucleus.

demonstrate that OE of LmnB1 at the NE prevents proper heterochromatin organization within the nucleus.

Lamin B1 overexpression does not induce a senescence phenotype

Since LmnB1 OE is not associated with senescence in cells that express hTERT [29], we wanted to directly test whether the observed changes in chromatin organization were forming independently from senescence. To address this, we first analyzed potential similarities between the DNA foci we observed in our system and senescence associated heterochromatin foci (SAHF), which have been shown to form in senescent cells [5,55,56]. Previously, we presented colocalization between the DNA foci and H3K9me3, which is one marker of SAHF (Figure 1a). Therefore, we tested the other markers of SAHF, including HP1α, H3K9me2, and H3K27me3. We observed colocalization between the DNA foci and HP1α in ~86% (42/49) of the nuclei, but no colocalization with H3K9me2 (Figure 2a, 2b Figure S2A, S2B). Additionally, we did not observe any major localization changes in H3K27me3, which has been shown to form a ring around the H3K9me3 core in SAHF [55] (Figure 2c).

We also monitored senescence induction at 9 days post LmnB1 OE using the CellEvent senescence green detection kit. In parallel, we treated RPE1 cells with doxorubicin to show positive induction of senescence in our system. In agreement with previous findings, we did not observe any senescent cells upon LmnB1 OE (Supplemental Figure S3) [29]. Taken together, this suggests that the DNA foci induced upon LmnB1 OE in our system are independent of senescence and are unique from SAHF.

Lamin B1 overexpression affects the tethering of peripheral heterochromatin

To understand how LmnB1 OE alters peripheral heterochromatin localization, we first asked whether these changes represent a defect in the targeting or tethering of heterochromatin at the NP. Since heterochromatin must be repositioned to the NP after every cell division, we assessed whether LmnB1 OE can still elicit the same changes in heterochromatin organization without mitosis. To test this, we first arrested cells in G1/S phase with aphidicolin, followed by doxycycline induction of LmnB1 OE. Using immunofluorescence imaging, we observed the formation of DNA foci colocalizing with H3K9me3 in more than 55% of arrested cells overexpressing LmnB1 (Figure 3). The lack of fluorescence signal from the thymidine analog EdU confirms that these cells did not undergo DNA synthesis while LmnB1 was being overexpressed. This demonstrates the independence of our observed phenotype from chromatin reorganization associated with mitosis and suggests that LmnB1 OE might compromise the tethering of heterochromatin at the NP in intact nuclei.

Since heterochromatin tethering is known to be mediated by NE-associated proteins, we assessed whether these proteins may be perturbed by LmnB1 OE. We monitored the localization and expression of classic NE-associated heterochromatin anchors, including Lamin A, Lap2, and Lamin B Receptor (LBR). However, we did not observe any changes in the localization or expression of these proteins (Supplemental Figure S4). Although a previous study reported a reduction in Lap2 expression and localization in an oligodendrocytic cell line (N20.1) upon LmnB1 OE, the authors also reported no changes in nuclear membrane components in a neuronal cell line (C17.2) and an astrocytic cell line (SVG p12) when LmnB1 is overexpressed [28]. This demonstrates that LmnB1 OE can affect components of the nuclear membrane in a cell type-specific manner. Further, this suggests that the changes in chromatin organization we observed in our system are not a consequence of altering the expression of these NE associated proteins.

Next, we tested whether changes in histone PTMs or their binding proteins may be implicated in the loss of peripheral heterochromatin upon LmnB1 OE. We assessed the global levels of H3K9me2 and H3K9me3, which are important PTMs for peripheral heterochromatin tethering, but did not observe significant changes by western blot (Figure 4a). Additionally, we monitored the levels of the H3K9me3 binding protein HP1α, but

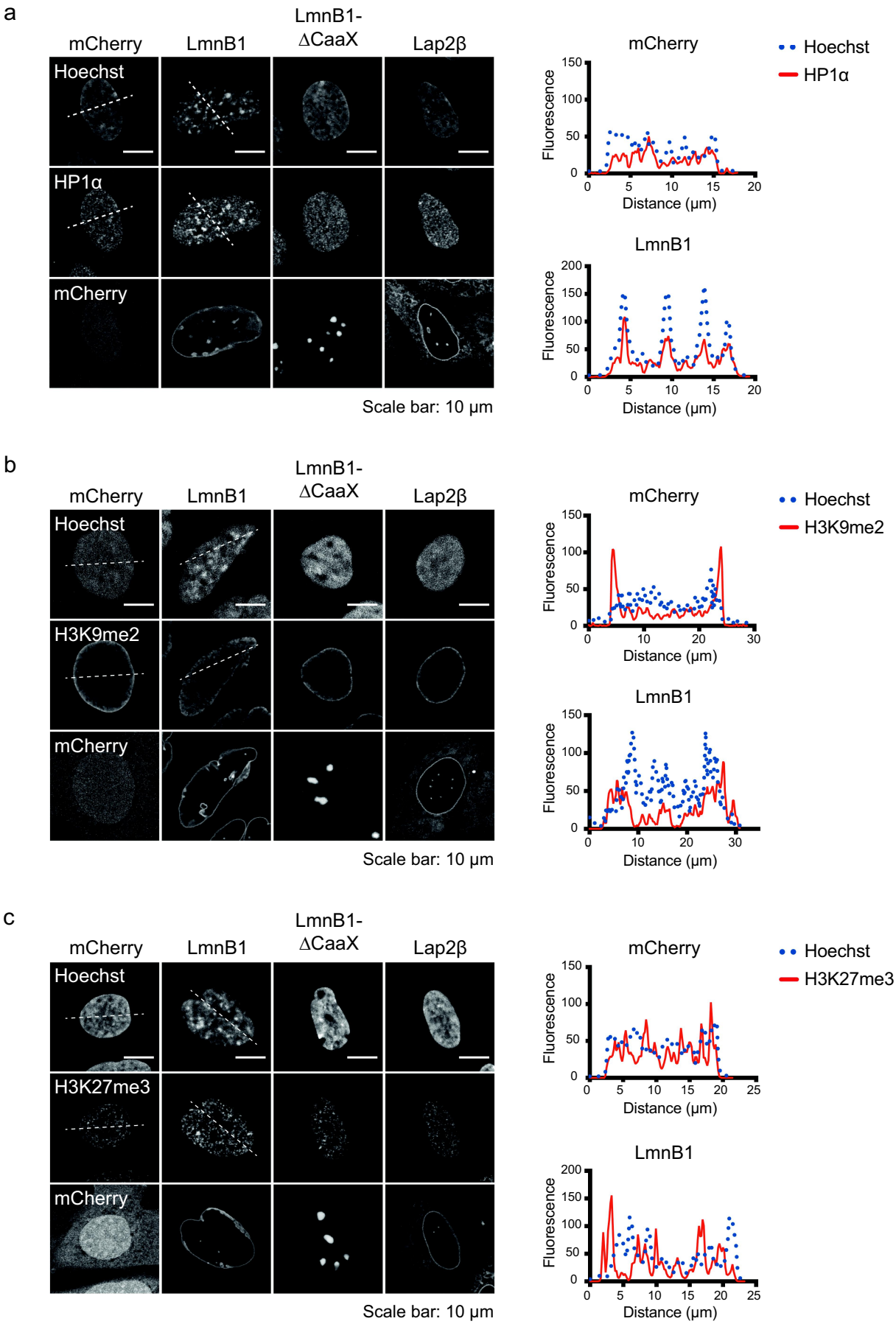

Figure 2. Lamin B1 overexpression induced DNA foci colocalize with HP1α, but not H3K9me2 or H3K27me3. Representative confocal images of RPE1 stable cell lines treated with doxycycline for 24 hours and labeled with (a) HP1α, (b) H3K9me2, and (c) H3K27me3.

did not see any loss that might affect the binding of heterochromatin at the periphery (Figure 4a).

Further, we used Cut&Run-sequencing with a H3K9me3-specific antibody to analyze any differences in the deposition of this PTM across the genome. However, we found that the H3K9me3 genomic-binding profiles were highly similar between cells overexpressing mCherry and LmnB1 (Figure 4b). Collectively, these results demonstrate that LmnB1 OE alters the tethering of heterochromatin at the NP through a mechanism independent from reducing the levels of NE-associated heterochromatin anchors or histone PTMs.

Lamin B1 overexpression alters gene expression

We next wanted to assess whether the dramatic changes in chromatin organization driven by LmnB1 OE have consequences on gene expression. Using mRNA-sequencing, we identified 118 downregulated and 161 upregulated genes upon LmnB1 OE (Figure 5a; log2 fold change <−1 or >1). The misregulation of these genes did not correlate with altered levels of H3K9me3, suggesting that changes in gene localization may be influencing gene expression (Supplemental Figure S5A). To test this hypothesis, we evaluated whether the misregulated genes were likely peripherally localized prior to LmnB1 OE. We used proximity to H3K9me3 peaks identified using Cut&Run in our RPE1 stable cell lines, or LmnB1 domains identified using previously published LmnB1 DamID datasets in RPE1 cells, to suggest peripheral positioning [52]. This analysis indicated that a significant number of the downregulated and upregulated genes are near H3K9me3 peaks or LmnB1 domains (Figure 5b). Pairing this with the changes in H3K9me3 localization we observed by immunofluorescence (Figure 1a), we propose that the downregulated genes may become sequestered within the H3K9me3 DNA foci and repressed, while the upregulated genes may be more accessible to transcription within the nucleoplasm or aberrantly transcribed at the NP, leading to their translocation into the nucleoplasm. As for the misregulated genes that are not near H3K9me3 peaks or LmnB1 domains, we hypothesize that these may be affected by altered chromatin contacts that might be induced by the changes in chromatin organization. It is also possible that misregulation of these genes may be secondary consequences arising from gene misregulation within LmnB1 domains or H3K9me3 regions of the genome.

Next, we examined what types of genes are being misregulated upon LmnB1 OE. Using gene ontology biological process enrichment analysis, we observed a number of developmental pathways among the upregulated genes, but no significant enrichment within the downregulated genes (Supplemental Figure S5B). This type of enrichment suggests that LmnB1 OE and the changes in chromatin organization may lead to the upregulation of genes that are normally repressed in this cell type, while the downregulated genes may represent secondary effects of these changes in chromatin organization.

To address whether the upregulated genes encompass those that are normally repressed, we first categorized ‘de-repressed genes’ as those with less than 100 mRNA counts in our control mCherry cell lines but showing upregulation upon LmnB1 OE. Using these parameters, we identified 179 de-repressed genes, 119 of which showed over twofold upregulation (Figure 5a; Supplemental Table S1). Thus, approximately 74% of the upregulated genes were previously silent or considerably repressed in our control cells. Again, these genes did not have altered levels of H3K9me3, but a significant number of genes were near H3K9me3 peaks or LmnB1 domains (Figure 5B; Supplemental Figure S5A). Gene ontology biological process enrichment analysis also showed a similar enrichment for various developmental pathways that should not be expressed in this cell type (Figure 5C; Supplemental Table S2). Collectively, this supports our hypothesis that LmnB1 OE is associated with

Single z slices through the center of the nucleus are shown. Plot profiles on the right illustrate the overlap of fluorescence signal between DNA (Hoechst) and HP1α, H3K9me2, or H3K27me3 over the white dotted lines in the mCherry and LmnB1 stable cell line images. In cells overexpressing LmnB1, the induced DNA foci colocalized with HP1α in 42/49 nuclei but did not colocalize with either H3K9me2 or H3K27me3 in > 50 nuclei.

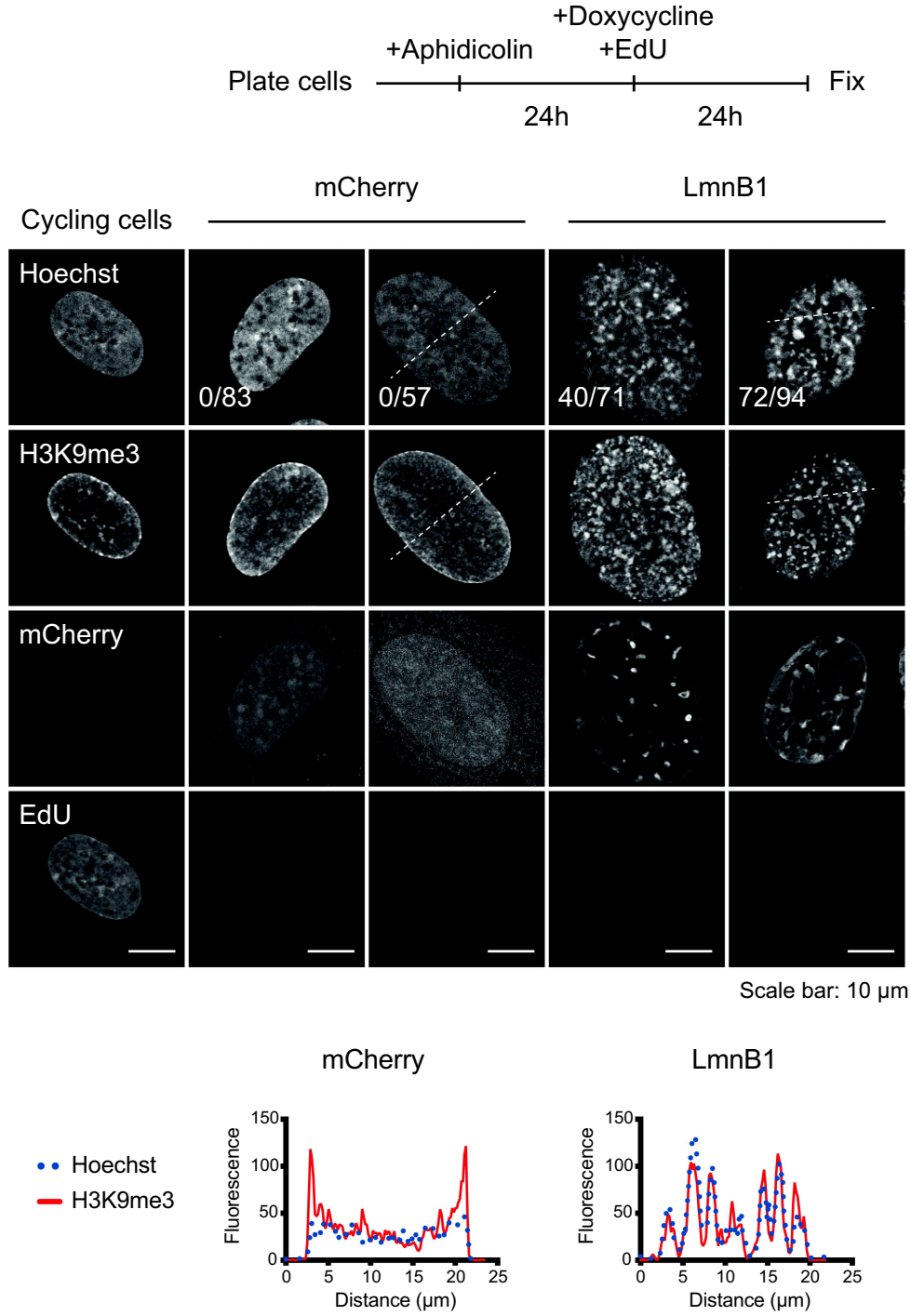

Figure 3. Lamin B1 overexpression induced changes in chromatin organization do not depend on mitosis. RPE1 stable cell lines were arrested with aphidicolin, followed by incubation with doxycycline and EdU, as depicted in the schematic at the top. Representative confocal images of H3K9me3 localization and EdU incorporation are displayed for two clonal cell lines per OE construct. Single z slices through the center of the nucleus are shown. Plot profiles at the bottom illustrate the overlap of fluorescence signal between DNA (Hoechst) and H3K9me3 over the white dotted lines in the mCherry and LmnB1 stable cell line images. The fraction represents the number of cells with intranuclear DNA foci over the total number of cells analyzed. Further, amongst the cells overexpressing LmnB1 with intranuclear DNA foci (40 nuclei and 72 nuclei), all exhibited colocalization with H3K9me3.

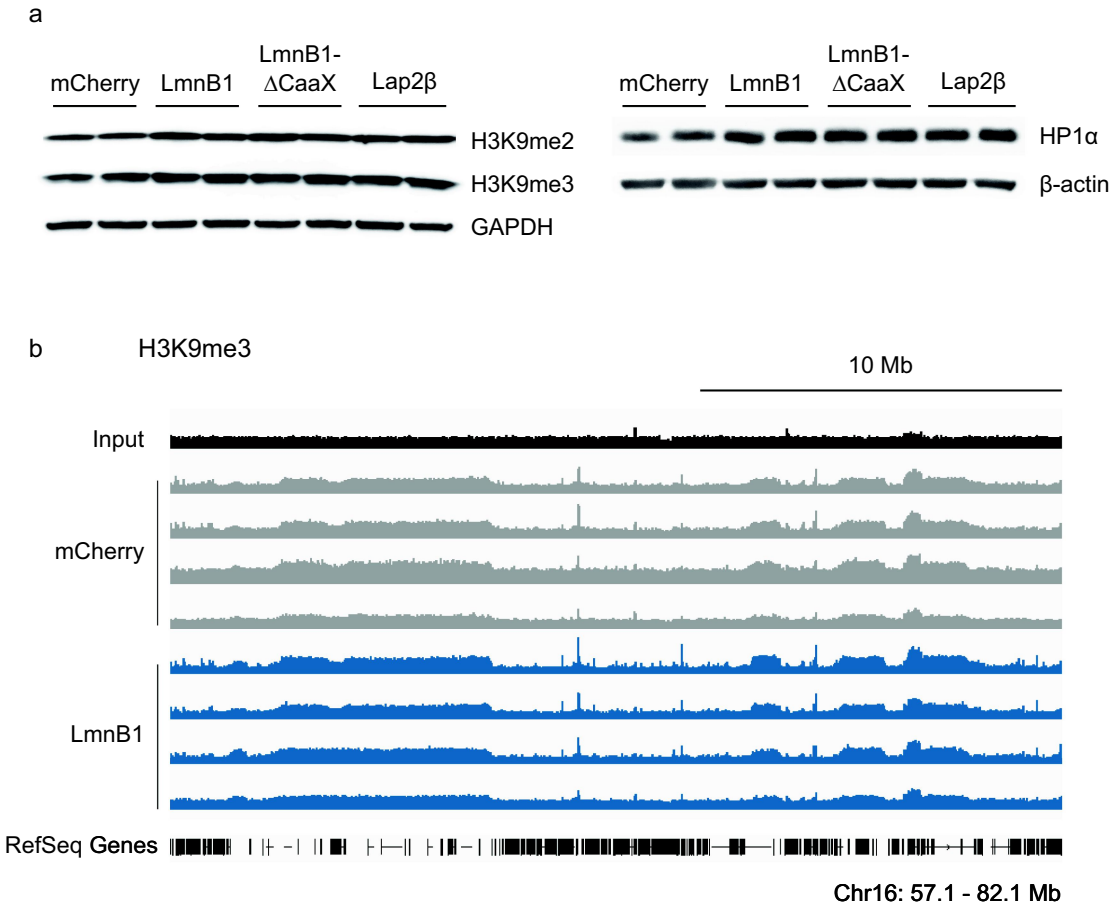

Figure 4. Lamin B1 overexpression induced changes in chromatin organization do not depend on altering the levels or deposition of H3K9me3. (a) RPE1 stable cell lines were treated with doxycycline for 24 hours and prepared for western blot analysis of H3K9me2, H3K9me3, and HP1α levels. Blots include two clonal cell lines for each OE construct. (b) Representative genome tracks of H3K9me3 deposition identified by Cut&Run sequencing. A 25 Mb region (57.1–82.1 Mb) on human chromosome 16 (hg38) is shown.

gene de-repression, and further suggests a broader consequence of LmnB1 OE on cell fate.

Altogether, our study highlights the significance of maintaining proper levels of LmnB1 for both chromatin organization and gene expression regulation. However, much remains to be explored regarding the mechanisms through which varying levels of LmnB1 affect these processes. Since LmnB1 OE alters peripheral heterochromatin localization without perturbing the expression of known heterochromatin adaptors, tethers, and histone PTMs important for heterochromatin anchoring at the NP, we speculate that LmnB1 OE may lead to the aberrant enrichment of LmnB1 interacting proteins at the NE that disrupt heterochromatin binding [57]. These might include histone methyltransferases or acetyltransferases that deposit active histone marks, leading to transcription or chromatin decompaction within these peripheral heterochromatic regions and their mislocalization away from the NP.

As for the changes in gene expression, we predict that these are impacted, at least in part, by altered chromatin organization in cells overexpressing LmnB1. Aberrant chromatin organization may lead to changes in gene localization, chromatin accessibility, and chromatin contacts, all of which may alter transcriptional output. It will be important to assess these changes using DNA fluorescence *in situ* hybridization, the assay for transposase-accessible chromatin with sequencing

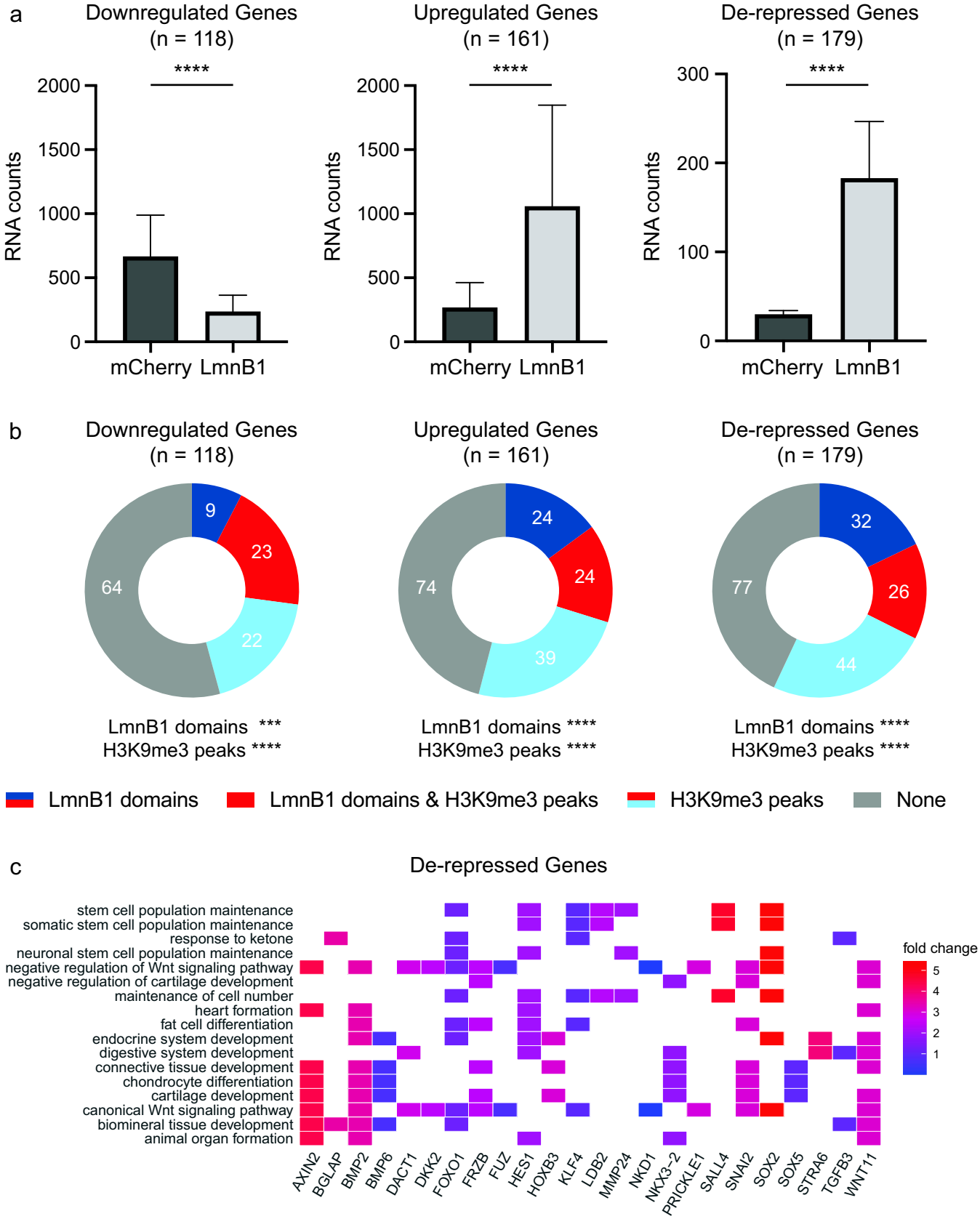

Figure 5. Lamin B1 overexpression alters gene expression. (a) mRNA counts (normalized) for the downregulated, upregulated, and de-repressed genes in RPE1 stable cell lines treated with doxycycline for 24 hours. Mean+95% confidence interval is plotted. Mann Whitney test for statistical significance: **** $p < 0.0001$. (b) Pie charts representing the number of downregulated, upregulated, and de-repressed genes that are near LmnB1 domains, H3K9me3 peaks, both LmnB1 domains and H3K9me3 peaks, or neither. Hypergeometric test for statistical significance of overlap between differentially expressed genes with LmnB1 peaks or H3K9me3 peaks: *** $p < 0.001$, **** $p < 0.0001$. (c) Gene ontology biological processes enrichment analysis for the genes de-repressed upon LmnB1 OE, with fold change for individual genes shown.

(ATAC-seq), and Hi-C, to better understand the correlation between altered chromatin organization and gene expression.

It will also be important to monitor the gain or loss of other histone PTMs, as alluded to earlier, since this has the potential to impact gene expression. Aberrant deposition of histone PTMs may be caused by LmnB1 OE itself, or LmnB1 OE-induced changes in chromatin organization. It will be interesting to further investigate global changes in active histone PTMs, since we observed a much clearer induction of genes upon LmnB1 OE. However, assessing the potential loss of heterochromatin markers, such as H4K20me, will also be important to include in this analysis. Cut&Run-sequencing can then be used to look at the deposition of specific histone PTMs across the genome to determine if they play a role in LmnB1 OE mediated changes in gene expression.

Collectively, our findings open new avenues for future research directions that will deepen our understanding of how LmnB1 OE alters chromatin organization and gene expression. These discoveries may also have broader applications in the context of diseases with elevated levels of LmnB1, such as a subset of cancers and neurological diseases [27,30–35]. LmnB1 OE has recently been shown to perturb telomere stability and the response to DNA damage, and our study describes additional misregulated processes that may also impact cellular homeostasis [58,59]. Therefore, LmnB1 expression must be properly regulated and understanding the consequences of LmnB1 OE represents an interesting field for further investigation.

Acknowledgments

We thank members of the Hetzer lab for critical review of the manuscript; Novogene for mRNA library preparation and sequencing; the Next-Generation Sequencing Core Facility at the Salk Institute, with funding from NIH-NCI CCSG: P30 014195, the Chapman Foundation, and the Helmsley Charitable Trust, for sequencing Cut&Run libraries; and the Waitt Advanced Biophotonics Core Facility at the Salk Institute, with funding from NIH-NCI CCSG: P30 014195, the Waitt Foundation, and the Chan-Zuckerberg Initiative Imaging Scientist Award, for electron microscopy sample preparation and imaging.

Disclosure statement

No potential conflict of interest was reported by the authors.

Funding

The work was supported by the Glenn Foundation for Medical Research [none]; Salk Women & Science [none]; NIH [R24GM13720]; NIH-NCI CCSG [P30 014195]

References

[1] Misteli T. Beyond the sequence: cellular organization of genome function. Cell. 2007;128:787–800.
[2] Di Micco R, Sulli G, Dobreva M, et al. Interplay between oncogene-induced DNA damage response and heterochromatin in senescence and cancer. Nat Cell Biol. 2011;13:292–302.
[3] Goldman RD, Shumaker DK, Erdos MR, et al. Accumulation of mutant lamin a causes progressive changes in nuclear architecture in Hutchinson-Gilford progeria syndrome. Proc Natl Acad Sci U S A. 2004;101:8963–8968.
[4] McCord RP, Nazario-Toole A, Zhang H, et al. Correlated alterations in genome organization, histone methylation, and DNA-lamin A/C interactions in Hutchinson-Gilford progeria syndrome. Genome Res. 2013;23:260–269.
[5] Narita M, Nũnez S, Heard E, et al. Rb-mediated heterochromatin formation and silencing of E2F target genes during cellular senescence. Cell. 2003;113:703–716.
[6] Solovei I, Kreysing M, Lanctôt C, et al. Nuclear architecture of rod photoreceptor cells adapts to vision in mammalian evolution. Cell. 2009;137:356–368.
[7] Chang L, Li M, Shao S, et al. Nuclear peripheral chromatin-lamin B1 interaction is required for global integrity of chromatin architecture and dynamics in human cells. Protein Cell. 2022;13:258–280.
[8] Goldberg M, Harel A, Brandeis M, et al. The tail domain of lamin Dm0 binds histones H2A and H2B. Proc Natl Acad Sci U S A. 1999;96:2852–2857.
[9] Harr JC, Luperchio TR, Wong X, et al. Directed targeting of chromatin to the nuclear lamina is mediated by chromatin state and A-type lamins. J Cell Bio. 2015;208:33–52.
[10] Malhas A, Lee CF, Sanders R, et al. Defects in lamin B1 expression or processing affect interphase chromosome position and gene expression. J Cell Bio. 2007;176:593–603.

[11] Poleshko A, Mansfield KM, Burlingame CC, et al. The human protein PRR14 tethers heterochromatin to the nuclear lamina during interphase and mitotic exit. Cell Rep. 2013;5:292–301.
[12] Solovei I, Wang AS, Thanisch K, et al. LBR and lamin A/C sequentially tether peripheral heterochromatin and inversely regulate differentiation. Cell. 2013;152:584–598.
[13] Taniura H, Glass C, Gerace L. A chromatin binding site in the tail domain of nuclear lamins that interacts with core histones. J Cell Bio. 1995;131:33–44.
[14] Wong X, Hoskins VE, Melendez-Perez AJ, et al. Lamin C is required to establish genome organization after mitosis. Genome Biol. 2021;22:305.
[15] Zullo JM, Demarco IA, Piqué-Regi R, et al. DNA sequence-dependent compartmentalization and silencing of chromatin at the nuclear lamina. Cell. 2012;149:1474–1487.
[16] Biferali B, Bianconi V, Perez DF, et al. Prdm16-mediated H3K9 methylation controls fibro-adipogenic progenitors identity during skeletal muscle repair. Sci Adv. 2021;7:eabd9371.
[17] Robson MI, de Las Heras JI, Czapiewski R, et al. Nuclear membrane proteins enhances repression of critical developmental genes during myogenesis. Mol Cell. 2016;62:834–847.
[18] Zuleger N, Boyle S, Kelly DA, et al. Specific nuclear envelope transmembrane proteins can promote the location of chromosomes to and from the nuclear periphery. Genome Biol. 2013;14:R14.
[19] Bian Q, Khanna N, Alvikas J, et al. β-Globin cis-elements determine differential nuclear targeting through epigenetic modifications. J Cell Bio. 2013;203:767–783.
[20] Kind J, Pagie L, Ortabozkoyun H, et al. Single-cell dynamics of genome-nuclear lamina interactions. Cell. 2013;153:178–192.
[21] Towbin BD, González-Aguilera C, Sack R, et al. Stepwise methylation of histone H3K9 positions heterochromatin at the nuclear periphery. Cell. 2012;150:934–947.
[22] Montavon T, Shukeir N, Erikson G, et al. Complete loss of H3K9 methylation dissolves mouse heterochromatin organization. Nat Commun. 2021;12:4359.
[23] Nicetto D, Donahue G, Jain T, et al. H3k9me3-heterochromatin loss at protein-coding genes enables developmental lineage specification. Science. 2019;363:294–297.
[24] Rao RA, Ketkar AA, Kedia N, et al. KMT1 family methyltransferases regulate heterochromatin-nuclear periphery tethering via histone and non-histone protein methylation. EMBO Rep. 2019;20:e43260.
[25] Brueckner L, Zhao PA, van Schaik T, et al. Local rewiring of genome-nuclear lamina interactions by transcription. Embo J. 2020;39:e103159.
[26] Therizols P, Illingworth RS, Courilleau C, et al. Chromatin decondensation is sufficient to alter nuclear organization in embryonic stem cells. Science. 2014;346:1238–1242.
[27] Barascu A, Le Chalony C, Pennarun G, et al. Oxidative stress induces an ATM-independent senescence pathway through p38 MAPK-mediated lamin B1 accumulation. Embo J. 2012;31:1080–1094.
[28] Lin ST, Fu YH. MiR-23 regulation of lamin B1 is crucial for oligodendrocyte development and myelination. Dis Model Mech. 2009;2:178–188.
[29] Dreesen O, Chojnowski A, Ong PF, et al. Lamin B1 fluctuations have differential effects on cellular proliferation and senescence. J Cell Bio. 2013;200:605–617.
[30] Alcalá-Vida R, Garcia-Forn M, Castany-Pladevall C, et al. Neuron type-specific increase in lamin B1 contributes to nuclear dysfunction in Huntington's disease. EMBO Mol Med. 2021;13:e12105.
[31] Coradeghini R, Barboro P, Rubagotti A, et al. Differential expression of nuclear lamins in normal and cancerous prostate tissues. Oncol Rep. 2006;15:609–613.
[32] Li W, Li X, Li X, et al. Lamin B1 overexpresses in lung adenocarcinoma and promotes proliferation in lung cancer cells via AKT pathway. Onco Targets Ther. 2020;13:3129–3139.
[33] Padiath QS, Saigoh K, Schiffmann R, et al. Lamin B1 duplications cause autosomal dominant leukodystrophy. Nat Genet. 2006;38:1114–1123.
[34] Radspieler MM, Schindeldecker M, Stenzel P, et al. Lamin-B1 is a senescence-associated biomarker in clear-cell renal cell carcinoma. Oncol Lett. 2019;18:2654–2660.
[35] Sun S, Xu MZ, Poon RT, et al. Circulating Lamin B1 (LMNB1) biomarker detects early stages of liver cancer in patients. J Proteome Res. 2010;9:70–78.
[36] Schafer ST, Paquola ACM, Stern S, et al. Pathological priming causes developmental gene network heterochronicity in autistic subject-derived neurons. Nat Neurosci. 2019;22:243–255.
[37] Lam SS, Martell JD, Kamer KJ, et al. Directed evolution of APEX2 for electron microscopy and proximity labeling. Nat Methods. 2015;12:51–54.
[38] Kopylova E, Noé L, Touzet H. SortMeRNA: fast and accurate filtering of ribosomal RNAs in metatranscriptomic data. Bioinformatics. 2012;28:3211–3217.
[39] Dobin A, Davis CA, Schlesinger F, et al. STAR: ultrafast universal RNA-seq aligner. Bioinformatics. 2013;29:15–21.
[40] Patro R, Duggal G, Love MI, et al. Salmon provides fast and bias-aware quantification of transcript expression. Nat Methods. 2017;14:417–419.
[41] Love MI, Huber W, Anders S. Moderated estimation of fold change and dispersion for RNA-seq data with DESeq2. Genome Biol. 2014;15:550.
[42] Yu G, Wang LG, Han Y, et al. clusterProfiler: an R package for comparing biological themes among gene clusters. OMICS. 2012;16:284–287.

[43] Li H, Durbin R. Fast and accurate short read alignment with burrows-wheeler transform. Bioinformatics. 2009;25:1754–1760.
[44] Amemiya HM, Kundaje A, Boyle AP. The ENCODE blacklist: identification of problematic regions of the genome. Sci Rep. 2019;9:9354.
[45] Amendola M, van Steensel B. Nuclear lamins are not required for lamina-associated domain organization in mouse embryonic stem cells. EMBO Rep. 2015;16:610–617.
[46] Ramírez F, Ryan DP, Grüning B, et al. deepTools2: a next generation web server for deep-sequencing data analysis. Nucleic Acids Res. 2016;44:W160–165.
[47] Stovner EB, Sætrom P, Hancock J. Epic2 efficiently finds diffuse domains in ChIP-seq data. Bioinformatics. 2019;35:4392–4393.
[48] Ross-Innes CS, Stark R, Teschendorff AE, et al. Differential oestrogen receptor binding is associated with clinical outcome in breast cancer. Nature. 2012;481:389–393.
[49] Heinz S, Benner C, Spann N, et al. Simple combinations of lineage-determining transcription factors prime cis-regulatory elements required for macrophage and B cell identities. Mol Cell. 2010;38:576–589.
[50] Yu G, Wang LG, He QY. ChIPseeker: an R/Bioconductor package for ChIP peak annotation, comparison and visualization. Bioinformatics. 2015;31:2382–2383.
[51] Liao Y, Smyth GK, Shi W. The R package Rsubread is easier, faster, cheaper and better for alignment and quantification of RNA sequencing reads. Nucleic Acids Res. 2019;47:e47.
[52] van Schaik T, Vos M, Peric-Hupkes D, et al. Cell cycle dynamics of lamina-associated DNA. EMBO Rep. 2020;21:e50636.
[53] Quinlan AR, Hall IM. Bedtools: a flexible suite of utilities for comparing genomic features. Bioinformatics. 2010;26:841–842.
[54] Alfonso P, Cañamero M, Fernández-Carbonié F, et al. Proteome analysis of membrane fractions in colorectal carcinomas by using 2D-DIGE saturation labeling. J Proteome Res. 2008;7:4247–4255.
[55] Chandra T, Kirschner K, Thuret JY, et al. Independence of repressive histone marks and chromatin compaction during senescent heterochromatic layer formation. Mol Cell. 2012;47:203–214.
[56] Zhang R, Chen W, Adams PD. Molecular dissection of formation of senescence-associated heterochromatin foci. Mol Cell Biol. 2007;27:2343–2358.
[57] Wong X, Cutler JA, Hoskins VE, et al. Mapping the micro-proteome of the nuclear lamina and lamina-associated domains. Life Sci Alliance. 2021;4:e202000774.
[58] Etourneaud L, Moussa A, Rass E, et al. Lamin B1 sequesters 53BP1 to control its recruitment to DNA damage. Sci Adv. 2021;7:eabb3799.
[59] Pennarun G, Picotto J, Etourneaud L, et al. Increase in lamin B1 promotes telomere instability by disrupting the shelterin complex in human cells. Nucleic Acids Res. 2021;49:9886–9905.